

Published in final edited form as:

Neuroimage. 2013 November 1; 81: 325–334. doi:10.1016/j.neuroimage.2013.05.038.

Visual callosal topography in the absence of retinal input

Andrew S. Bock^a, Melissa Saenz^b, Rosalia Tungaraza^c, Geoff M. Boynton^a, Holly Bridge^d, and Ione Fine^a

^aDepartment of Psychology, University of Washington, Seattle, WA 98195, USA ^bDepartment of Clinical Neuroscience, University of Lausanne, 1011 Lausanne, Switzerland ^cIntegrated Brain Imaging Center (IBIC), Department of Radiology, University of Washington, Seattle, WA 98195, USA ^dFMRIB Centre, Clinical Neurosciences, University of Oxford, Oxford, OX3 9DU, United Kingdom

Abstract

Using probabilistic diffusion tractography, we examined the retinotopic organization of splenial callosal connections within early blind, anophthalmic, and control subjects. Early blind subjects experienced prenatal retinal “waves” of spontaneous activity similar to those of sighted subjects, and only lack postnatal visual experience. In anophthalmia, the eye is either absent or arrested at an early prenatal stage, depriving these subjects of both pre- and postnatal visual input. Therefore, comparing these two groups provides a way of separating the influence of pre- and postnatal retinal input on the organization of visual connections across hemispheres. We found that retinotopic mapping within the splenium was not measurably disrupted in early blind or anophthalmic subjects compared to visually normal controls. No significant differences in splenial volume were observed across groups. No significant differences in diffusivity were found between early blind subjects and sighted controls, through some differences in diffusivity were noted between anophthalmic subjects and controls. These results suggest that neither prenatal retinal activity nor postnatal visual experience play a role in the large-scale topographic organization of visual callosal connections within the splenium.

Keywords

development; blind; anophthalmia; tractography; plasticity; diffusion tensor imaging

1. Introduction

Visual deprivation is a classic paradigm for studying organization and plasticity in the central nervous system within both animals and humans (Wiesel and Hubel, 1965a, b). The visual system is relatively well-understood and at least a fifth of the brain is normally devoted to visual processing, thereby offering the opportunity to study large-scale reorganization during development. Here we use blindness to examine the role of pre- and

© 2013 Elsevier Inc. All rights reserved.

Corresponding author: Andrew S. Bock, Ph.D. Department of Psychology University of Washington Seattle, WA 98195 Tel: 206.543.3817 Fax: 206.685.3157 abock@u.washington.edu.

Publisher's Disclaimer: This is a PDF file of an unedited manuscript that has been accepted for publication. As a service to our customers we are providing this early version of the manuscript. The manuscript will undergo copyediting, typesetting, and review of the resulting proof before it is published in its final citable form. Please note that during the production process errors may be discovered which could affect the content, and all legal disclaimers that apply to the journal pertain.

postnatal neural activity on the large scale organization of fibers within the corpus callosum in humans.

In many species (including humans), the right visual cortex represents the left side of the visual field and the left visual cortex represents the right visual field. These two halves are interconnected via axonal projections that pass through the splenium at the posterior end of the corpus callosum (Clarke and Miklossy, 1990; de Lacoste et al., 1985; Pandya et al., 1971; Rockland and Lund, 1983) allowing for coverage of the visual field across the vertical meridian. Although organization within the callosum is difficult to systematically map using electrophysiology techniques, studies in the cat (Hubel and Wiesel, 1967) and monkey (Rockland and Pandya, 1986) have found some evidence for topographic organization of visual fibers within the splenium itself. In humans, Dougherty et al. (2005) found dorsal-to-ventral organization within splenial fibers projecting from early visual areas (V1/V2, V3, V3A/B, V4 and V7). More recently, Saenz & Fine (2010) further demonstrated organization based on eccentricity. Visual inspection of the maps suggested that fibers connecting dorsal visual areas were clustered in the superior-caudal region of the splenium, while fibers connecting ventral visual areas were clustered in the inferior-rostral corner of the splenium. In the case of eccentricity, projections from foveal-to-peripheral V1 sub-regions appeared to map from the superior-rostral to the inferior-caudal direction within the splenium: orthogonal to the dorsal-to-ventral mapping.

While input from the retina influences the organization of cortical connections at the level of cortex (Goodman and Shatz, 1993; Katz and Crowley, 2002; Katz and Shatz, 1996; Lopez-Bendito and Molnar, 2003; Price et al., 2006; Sur and Rubenstein, 2005), it is less clear the degree to which retinal input affects the development and/or maintenance of fibers within the cortical white matter fiber tracts themselves. Some studies (Lepore et al., 2010; Levin et al., 2010) suggest that early postnatal blindness leads to a reduction in splenial white matter volume, however, Bridge et al. (2009) did not find any structural differences within the splenium between anophthalmic subjects and their matched control subjects. Similarly, one of the first studies to use diffusion-weighted imaging to investigate the developmental effects of sensory deprivation by Shimony et al. (2006) found a reduction in fractional anisotropy between early blind subjects and sighted controls (interestingly, Bridge et al. (2009) found somewhat different results using a smaller group of anophthalmic subjects).

Here, using T1- and diffusion-weighted imaging combined with diffusion based probabilistic tractography, we examined the volume, diffusivity, and topographic organization of visual callosal connections within normally-sighted, early blind, and anophthalmic subjects. Early blind subjects, who lost vision from birth to the first 5 years of life, experienced prenatal retinal “waves” of spontaneous activity prior to losing sight, and only lack postnatal visual experience. In anophthalmia, the input from the optic nerves to the thalamus and midbrain never exists (or only exists temporarily, early in development before the embryonic eyes degenerate (Stevenson, 2006)). As a result, anophthalmic subjects not only lack postnatal visual experience, but also do not experience (or have much reduced) prenatal retinal “waves” of spontaneous activity as compared to sighted and early blind humans. Comparing these groups offers a way of at least partially separating the influence of pre- and postnatal retinal input on the retinotopic organization of visual connections across hemispheres, and provides an important addition to literature investigating the influence of neuronal activity on the development and maintenance of retinotopic connections between visual hemispheres that has thus far been entirely confined to animal models (Chalupa, 2009; Graven, 2004; Huberman et al., 2005).

Several studies have examined the effect of visual deprivation on callosal connections, with somewhat inconsistent findings (Bridge et al., 2009; Lepore et al., 2010; Levin et al., 2010;

Shimony et al., 2006), as described below. Our study is unique in examining the effect of blindness on the retinotopic organization of splenial connections. We find that visual callosal fibers are retinotopically organized in sighted controls, as shown previously (Dougherty et al., 2005; Saenz and Fine, 2010), and that this organization is preserved in both early blind and anophthalmic subjects. These results suggest that the gross retinotopic organization of visual fibers within the splenium develops and is maintained independently from any pre- or postnatal retinal input, and that changes as a result of blindness in this pathway may occur as white matter connections innervate cortex, rather than within the tracts themselves.

2. Materials and methods

2.1. Subjects

Six anophthalmic subjects (two females, mean age 24.2 \pm 5.2), six early blind subjects (three females, mean age 49.5 \pm 13.4) (see **Table 1**), and 15 normally-sighted control subjects (eight females, mean age 27.7 \pm 4.6) participated. Note that the average age of early blind subjects is larger than for the other two groups. However a 2-way ANOVA (subject group \times diffusivity measure: FA, MD, L1, L23, see below) performed on the Fisher's r to z transform of the correlation between age and diffusivity measures found no interaction between age and diffusivity values. All sighted subjects had normal or corrected-to-normal vision. All subjects provided informed written consent, and all procedures involved were approved by either the Oxfordshire NHS Research Ethics Committee (07/Q1605/20) or the Institutional Review Board at the University of Washington.

2.2. Data collection and analysis

Imaging of six control and all anophthalmic subjects was performed at the Oxford Centre for Clinical Magnetic Resonance using a Siemens 3T Trio scanner with a 12-channel head coil. Imaging of the remaining nine control and all early blind subjects was performed at the UW Medical Center using a Philips 3T scanner with an 8-channel head coil. Some of the data and results (though using slightly different analysis methods) obtained from the six control and anophthalmic subjects whose data were collected at Oxford have been previously reported (Bridge et al., 2009), as specified below.

At both centers high-resolution anatomical images were acquired using a standard 1mm³ T1-weighted magnetization prepared rapid gradient echo (MP-RAGE) sequence. Diffusion-weighted images were acquired axially using echoplanar imaging, with isotropic voxels of 2mm³. The diffusion weighting was isotropically distributed through space (Jones et al., 1999) along 60 directions using a b-value of 1000s/mm². For 1 early blind subject, diffusion weighting was distributed along 32 directions. The total acquisition time for both structural and diffusion data was ~30 min. All subsequent analysis of the data was conducted on the same workstation running Ubuntu 12.04. Analysis consisted of the following steps:

2.2.1. Definition of occipital ROIs on the cortical surface—Cortical reconstruction and volumetric segmentation was performed with the Freesurfer v5.1.0 image analysis suite, which is documented and freely available for download online (<http://surfer.nmr.mgh.harvard.edu/>). Briefly, this processing includes skull-stripping (Segonne et al., 2004), subcortical segmentation (Fischl et al., 2002; Fischl et al., 2004), intensity normalization (Sled et al., 1998), surface generation (Dale et al., 1999; Dale and Sereno, 1993; Fischl and Dale, 2000), topology correction (Fischl et al., 2001; Segonne et al., 2007), surface inflation (Fischl et al., 1999a), registration to a spherical atlas (Fischl et al., 1999b) and thickness calculation (Fischl and Dale, 2000).

Three sets of ROIs were then defined on the cortical surface:

2.2.1.1. Occipital lobe ROI: This ROI was chosen to include all early visual areas on the Freesurfer cortical surface using the Destrieux surface based atlas (Destrieux et al., 2010).

2.2.1.2. V1/V2 ROI: A surface-based estimate of the location of primary visual cortex (V1) from cortical folds was obtained using Freesurfer (Hinds et al., 2009; Hinds et al., 2008). As callosal connections in primate visual cortex are found at the highest density within a narrow zone straddling the V1/V2 border (Clarke and Miklossy, 1990; Kennedy et al., 1986; Van Essen et al., 1982), a V1/V2 ROI (larger than the V1 ROI used by Saenz and Fine, 2010) was drawn by expanding the border of V1 to the fundi of the lingual sulcus and the neighboring paracalcarine sulcus to ensure the inclusion of visual callosal connections on the V1/V2 border. As the exact width of the callosal projection zone is known to vary according to eccentricity, as well as species (Kennedy et al., 1986; Olavarria, 1996; Payne et al., 1991; Segraves and Rosenquist, 1982), we allowed our V1/V2 ROI to extend fully into the acallosal center of V1. The anterior border of the V1/V2 ROI was drawn at the posterior edge of cuneal cortex (defined using Destrieux surface based atlas (Destrieux et al., 2010)) and carried perpendicular to the calcarine sulcus to the ventral edge of the V1/V2 ROI (see **Figure 1**). Care was taken to draw these borders as consistently as possible, based on each subject's predicted V1 location and cortical folds, however due to the inherent variability in the gyrification of the human brain, some variability in the location of the borders between subjects was unavoidable.

2.2.1.3. Subregion V1/V2 ROIs: The V1/V2 ROI described above was further partitioned into five sub-regions: dorsal, ventral, anterior, middle, and posterior (see **Figure 1**). The dorsal and ventral sub-regions were located dorsal and ventral to the calcarine sulcus, respectively. Following the calcarine sulcus, the most posterior point in the V1/V2 ROI was chosen to divide the dorsal and ventral regions. The anterior, middle, and posterior sub-regions were drawn perpendicular to the calcarine sulcus as pseudo-rectangular regions of equal width within the V1/V2 ROI.

2.2.2. Co-registration of anatomical and diffusion space—Each subject's individual anatomical image was registered to that subject's respective diffusion-weighted images, which were corrected for eddy currents and head motion and skull-stripped, using FMRIB's software library and diffusion toolbox v2.0 (FSL, freely available at <http://www.fmrib.ox.ac.uk/fsl/>). The resulting registration matrices were used to transform the cortical surface ROIs described above to diffusion space. All cortical surface ROIs were projected 2mm into white matter from the grey/white matter boundary and transformed to three-dimensional subject-specific diffusion space for subsequent tractography analysis.

2.2.3. Generation of streamlines from the occipital ROI—Probabilistic tractography was performed in diffusion space using FMRIB's diffusion toolbox (FDT). Briefly, FSL-FDT repeatedly samples from the distribution of diffusion directions for each voxel that were generated through Bayesian estimation. Streamlines are generated from each voxel within the occipital ROI by drawing a line in the sampled direction towards the next voxel. Relatively standard parameters were used: number of diffusion directions modeled = up to 2/voxel, number of streamlines = 5000/voxel, curvature threshold = 0.2, maximum number of steps = 2000, and step length = 0.5mm (Behrens et al., 2007; Behrens et al., 2003a; Behrens et al., 2003b).

2.2.4. Restriction of streamlines from the occipital ROI

- a. Any fiber that passed through the midline posterior to the corpus callosum was excluded to prevent fibers from erroneously crossing into neighboring voxels across the hemispheric gap.
- b. Following methods described previously (Dougherty et al., 2007; Huang et al., 2005) an ROI was drawn to delineate occipital vs. parietal cortex (using the intersection of the calcarine and occipital-parietal sulcus as a boundary) within a single coronal slice at the anterior border of the occipital lobe. Only those fibers that pass through this ROI were retained, thereby excluding parietal-callosal fibers.
- c. A callosal region of interest was drawn on a single midline sagittal slice. Only those fibers that passed through this ROI were retained (and streamlines terminated at this ROI).

2.2.5. Identification of the splenium—We defined the splenium as including any voxel within the corpus callosum where at least 2500 tracts seeded from the occipital ROI terminated. Increasing the stringency of our threshold had only minor effects on the size of the splenial region until an extremely stringent criterion was used. Lowering the threshold gradually increased the size of the splenial region and clearly included voxels within the corpus callosum that were outside the splenium. Thus this threshold was chosen to maximize the number of reliably identified splenial voxels. Identification of the splenium using a smaller occipital ROI likely to be restricted to V1/V2 (for example, to the size of the ROI used by Saenz and Fine, 2010) results in a splenial ROI that is very similar in shape and location, although slightly smaller. Tracts coincided with the inferior-rostral boundary of the splenium in both subject-specific diffusion space and diffusion-registered anatomical space, indicating good registration between T1 and diffusion weighted images.

2.2.6. Calculation of projection probabilities—Fibers were seeded from this splenial ROI (using the same FDT parameters described above) and only those voxels in the seed region with a streamline connection probability of $p = 0.02$ (100 out of 5000 streamlines) were retained. The probability of a streamline connection with a V1/V2 subregion for each splenial voxel was evaluated as the proportion of the total number of streamlines reaching any subregion in that map (dorsal-to-ventral map or anterior-to-posterior map). For example, for a given splenial voxel, the streamline connection probability to the dorsal subregion was calculated by dividing the number of streamlines reaching the dorsal subregion by the number of streamlines reaching both dorsal and ventral subregions. As shown in **Figure 2A,B**, each voxel in the splenium was color-labeled in a graded fashion according to its proportional streamline connectivity to each of the target regions. The dorsal-to-ventral classification was labeled such that voxels primarily connected to the dorsal region were blue, and those primarily connected to the ventral region were green. The anterior-to-posterior classification was likewise labeled using a yellow-red scale.

2.2.7. Quantification of projection probabilities—The callosum of each subject was re-oriented such that a horizontal line passed through the most anterior point of the genu and the most posterior point of the splenium in a mid-sagittal slice. Each splenial probabilistic map was then fit with a linear ramp with free parameters quantifying the orientation (θ) and gradient (m) of the dorsal-to-ventral or anterior-to-posterior map, **Figure 2C,D**. These linear ramps can be described by a vector where the vector angle represents the orientation of the map and the vector line length represents the map gradient, in terms of the change in color/pixel (see overlay vectors on **Panels C and D**). **Figure 2E** shows the resulting vector plots for a single sighted subject, all subjects are shown in **Supplementary Figures 3-5**. If callosal connections are retinotopically organized then these vectors should be orthogonal.

3. Results

3.1. Volume and Diffusivity

3.1.1 Splenial volume—We used Freesurfer v5.1.0 volumetric segmentation to identify the corpus callosum, and this callosal volume ROI was translated into diffusion space. This volumetric definition of the corpus callosum spans several sagittal slices (5mm) and is therefore likely to be robust to small differences in acquisition orientation across individuals. For both the callosal and splenial volumes for each group, Lilliefors' test failed to reject the null hypothesis ($p > 0.05$) that the volume distributions are normal. Using a 1-factor ANOVA, we found no difference in either the volume of the corpus callosum or the volume of the splenium across groups. Nor was there a difference across groups in the ratio of the splenium to corpus callosum, (**Figure 3**, also see **Table 2**). Similar analyses were carried out using the cross-sectional area (of a single midline slice), and no significant differences across subject groups were observed (see **Table 2**). Previous groups have presented data (Levin et al., 2010) suggesting that binocular blindness may result in a reduction of the cross-sectional area of occipital-callosal fibers, however the authors note that the blind subject also had a small corpus callosum, and that the size of the occipital-callosal cross-section in relation to the size of the corpus callosum was similar to controls. Like Levin et al., we did find a positive correlation between the size of the corpus callosum and the size of the splenium across all subject groups (Control $R^2 = 0.31$; Early Blind $R^2 = 0.41$; Anophthalmic: $R^2 = 0.94$; $p = 0.57$). However, we saw no indication of a reduction in the size of the splenium or the corpus callosum in either early blind or anophthalmic subjects, as shown in **Figure 3**. The general finding of a lack of difference in the splenial and callosal volume between anophthalmic and control subjects (using different analysis methods) based on the same anophthalmic dataset has been previously reported (Bridge et al., 2009).

3.1.2 No evidence of reduced numbers of streamlines across groups—We saw no evidence of atrophy of visual-callosal connections based on the number of streamlines. Fibers seeded in the splenial mask reached a V1/V2 target mask in either hemisphere with an equal probability for all groups (Control Mean: 33.48 \pm 11%; Early Blind Mean: 27.12 \pm 14%; Anophthalmic Mean: 22.10 \pm 8%; $p = 0.13$).

3.1.3 Diffusivity—Note that in all the diffusivity analyses of **Table 3** (see also **Supplementary Figure 2**), anophthalmic and early blind subjects were compared to control subjects whose data were acquired on the same scanner, as different scanners produce slightly different diffusivity measurements (Takao et al., 2011). There was no difference in fractional anisotropy across groups within either callosal or splenial volumes. The lack of a difference in splenial fractional anisotropy between anophthalmic and control subjects (using different analysis methods) has been previously reported (Bridge et al., 2009).

We found reduced longitudinal (L_1) and radial diffusivity (L_{23}) within the splenium in anophthalmic subjects. Two types of post-hoc multiple comparison correction were carried out: Bonferroni-Holm (B-H) - a conservative method designed to control the family-wise error, and the less conservative false discovery rate (FDR based on a method by Benjamini & Hochberg (1995)) - designed to limit the number of false-negatives. The difference in longitudinal (L_1) diffusivity was not significant using B-H correction, but was significant at the $p < 0.05$ level using FDR correction. Differences in radial diffusivity (L_{23}) were not significant after correction using either procedure.

There was no difference in longitudinal (L_1) or radial diffusivity (L_{23}) within the callosal volumes across groups. There was higher mean diffusivity (MD) within the splenial volume in controls compared to anophthalmic subjects, this survived correction using both

procedures ($p < 0.01$ for both methods). There was no difference in mean diffusivity between early blind and sighted controls. We found no difference in mean diffusivity (MD) within the callosal volume across groups.

3.2. Topography

Figure 4 shows vector plots for all three subject groups. The blue lines represent the dorsal-to-ventral mapping; red lines represent the anterior-to-posterior mapping. The orientation and gradient values for each map across groups can be found in **Table 4**.

We saw evidence for clear orthogonality between dorsal-to-ventral and anterior-to-posterior maps, mirroring the orientation of the cortical subregions, across all three subject groups (**Figure 4**, right column), see also **Table 4**). Using the circular equivalent to a one-sample t-test (Bonferroni corrected for multiple comparisons) with a specified mean direction we found that the angular difference between these two maps was significantly different from 0 degrees for each group (Control: $p = 0.001$; Early Blind: $p = 0.035$; Anophthalmic: $p = 0.018$), and was not significantly ($p > 0.05$) different from 90 degrees for each group. A parametric Watson-Williams multi-sample test for equal means showed no difference ($p = 0.78$) in map orthogonality across groups.

There was no rotation in the orientation of either the dorsal-to-ventral or anterior-to-posterior mapping in either early blind or anophthalmic subjects compared to sighted subjects. Statistical comparison by a parametric Watson-Williams multi-sample test for equal means (which can be considered as the equivalent of a one-way ANOVA for circular data), showed no difference in the orientation of either dorsal-to-ventral or anterior-to-posterior maps between groups. Nor did we see a difference in the gradient of the dorsal-to-ventral or anterior-to-posterior mapping in either early blind or anophthalmic compared to sighted subjects. A one-way ANOVA revealed no difference in the gradient of either the dorsal-to-ventral or anterior-to maps between any of the groups (see **Table 4**).

There was no evidence for greater variability within the maps of anophthalmic or early blind subjects compared to sighted subjects: Bartlett's test for equal variances showed the same degree of variability across groups for dorsal-to-ventral and anterior-to-posterior orientations and gradients. There was no difference in the R^2 values (describing the goodness of fit of the linear ramp as a model of topographic organization) across groups for either the dorsal-to-ventral (Control: 0.44; Early Blind: 0.37; Anophthalmic: 0.41; $p=0.57$) or anterior-to-posterior (Control: 0.35; Early Blind: 0.37; Anophthalmic: 0.37; $p=0.95$) maps, suggesting splenial fibers have a similar level of organization across groups. Finally, we carried out a bootstrap analysis comparing R^2 values from this fitting procedure to R^2 values obtained after randomly shuffling voxels of the each hemisphere's map. As expected, bootstrapped R^2 values for shuffled maps clustered near zero for both dorsal-to-ventral and anterior-to-posterior maps. For every subject, R-squared values for the dorsal-to-ventral and anterior-to-posterior maps were found to fall outside the 99% confidence interval for bootstrapped R^2 squared values from 'random maps'.

Although we did not observe any significant correlations between our orientation and gradient measures across all subjects, it is nonetheless possible that the relationship between these measures differed across blind and sighted subject groups. We examined this further by plotting, for example, dorsal-ventral orientation vs. anterior-posterior orientation, calculating the two standard deviation covariance ellipse based on sighted subjects only, and then counting the number of blind (collapsing across subject groups) subjects falling outside the ellipse. We used a Monte-Carlo procedure (assigning subject groups randomly on each iteration) to examine whether the number of blind subjects falling outside the ellipse was larger than might be predicted by chance. The only case in which a larger number of

subjects fell outside the ellipse than might be expected by chance was the comparison between dorsal-ventral and anterior-posterior orientations, and visual inspection of the data revealed no systematic difference between blind and sighted subjects in the pattern of data or the position of outliers. These data are shown in **Supplementary Figure 1**.

4. Discussion

Here we compared the volume, diffusivity, and topographic organization of visual callosal connections within normally-sighted, early blind, and anophthalmic subjects using T1- and diffusion-weighted imaging combined with diffusion based probabilistic tractography. We found no difference in the gross topographic organization of visual callosal connections across groups, despite the lack of prenatal retinal activity and/or postnatal visual experience, suggesting that retinal neuronal activity is not required for the development and maintenance of topography in these connections.

We did find reduced mean diffusivity and possibly reduced longitudinal diffusivity in anophthalmic subjects, but not early blind subjects, suggesting that while the gross organization of these tracts is robust to loss of visual experience, the loss of prenatal retinal input may affect the tissue properties of these tracts.

4.1 Comparison to previous studies: callosal and splenial volume

Across our 6 early blind, 6 anophthalmic subjects (these data were previously reported in Bridge et al., 2009) and 15 sighted controls we saw no evidence of either a reduction or expansion in the size of the corpus callosum, the size of the splenium, or proportion of the callosum containing visual splenial fibers. A previous study (Levin et al., 2010) compared the cross-sectional area of the splenium and corpus callosum in an early blind subject, a sight recovery subject (MM, blinded between the ages of 3.5 and 46), and 10 sighted controls. A comparison of the data re-plotted from Levin et al. (2010) with ours (**Supplementary Figure 6**) suggests that their data actually agrees with ours quite closely. While Levin et al.'s early blind subject had an abnormally small callosum, his ratio of his splenial/callosal cross-sections fell within the normal range and the reduction in callosal cross-sectional area may reflect normal subject variability. In contrast, the sight recovery subject MM had an abnormally large callosal area, and the ratio of his splenial/callosal cross-sections was abnormally small.

Lepore et al. (2010) using tensor-based morphometry, found a significant reduction of volume within rostral regions of the splenium (with nearby non-significant increases in volume within more caudal regions) across 16 early blind subjects as compared to 16 matched sighted controls. This Lepore study had a larger number of subjects in each group; however our results are not indicative of a failure to find volumetric differences within the splenium due to a lack of power. One significant difference in methodology is that the splenium was identified individually in each of our subjects. In contrast, Lepore et al. used tensor-based morphometry whereby a voxel-wise comparison is carried out after brains are nonlinearly aligned across subjects. However, there seems no obvious reason why the known anatomical differences between early blind and sighted subjects within occipital cortex (Dehay et al., 1996; Dehay et al., 1989; Jiang et al., 2009) would result in misregistration of the callosum across groups (Ashburner et al., 2000; Ashburner and Friston, 2001), though Lepore et al.'s finding of non-significant increases in neighboring callosal areas is consistent with such a possibility.

4.2 Comparison to previous studies: diffusivity

Previous studies using diffusion tensor imaging have suggested that early blindness leads to changes in diffusivity within the splenium. Levin et al. (2010) did not find any significant difference in fractional anisotropy or axial diffusivities within the splenium of their sight recovery subject. However, their early blind subject had lower fractional anisotropy and higher mean diffusivity than the 95% confidence interval of the sighted controls. Shimony et al. (2006) found no difference in mean diffusivity between 5 early blind subjects (3 ROP) and 7 seven sighted controls, but did find a reduction in A_{σ} , which is proportional to relative anisotropy, within blind subjects that was (barely) significant. Yu et al. (2007) found a significant reduction in fractional anisotropy within the splenium across 17 early blind subjects and their sighted controls.

We saw no differences in radial diffusivity or fractional anisotropy within the splenium or the corpus callosum between our sighted and anophthalmic and early blind subjects. We did find a slight reduction in mean diffusivity and possibly longitudinal diffusivity in the splenium of anophthalmic subjects compared to controls. This finding of no reduction of fractional anisotropy in anophthalmic subjects has been previously reported based on the same dataset (Bridge et al., 2009). The fractional anisotropy and mean diffusivity values for the early blind subject reported by Levin et al. (2010) are within the range of the values reported here, so the difference between their results and ours may be explained by variability across subjects, however comparing diffusivity values across scanners is problematic (Takao et al., 2011). It is not clear why our results differ from those of Shimony et al. (2006), however they measured relative anisotropy, compared to fractional anisotropy reported here. It is known that fractional anisotropy images have a higher signal-to-noise ratio and superior noise immunity compared to relative anisotropy (Hasan et al., 2004), which may explain the difference in our results. The difference between our results and those of Yu et al. (2007) may also be due to a difference in methodology. Yu et al. (2007) defined the splenium as the posterior quadrant of the corpus callosum in a midsagittal slice, which may have contained non-visual fibers both inside and outside the splenium, whereas our splenium was defined in individual subjects based on tracts from visual cortical areas, resulting in a volume that is slightly smaller. It is therefore possible that the differences found by Yu et al. (2007) are driven by regions of the callosal tract that fall outside the visual portion of the splenium. Thus, it is possible that blindness affects callosal diffusivity values in non-visual and/or multimodal callosal fibers, as also suggested by the finding of Bridge et al. (2009) of reduced FA in anterior portions of the callosum. This could be examined in future studies by examining diffusivity values between sighted and blind individuals using callosal ROIs defined by seeding from a wider variety of cortical areas (e.g. somatosensory, motor, auditory, prefrontal).

4.3 Comparison to previous studies: tract organization

Shimony et al. (2006) compared the size of white matter tracts in 5 early blind (3 due to retinopathy of prematurity) and 7 sighted subjects. Although some variability was observed across subjects, in all but one early blind subject the splenial tracts appeared grossly normal in appearance. A recent paper involving two achiasmic subjects (Hoffmann et al., 2012) similarly showed that despite atypical retinal input and highly abnormal functional responses in visual cortex, the gross topography of geniculostriate and occipital callosal connections remains largely unaltered.

Our paper is the first to examine how visual deprivation affects the topographical organization of fibers within the splenium itself. Like previous studies of sighted subjects (Dougherty et al., 2005; Saenz and Fine, 2010) we found that visual callosal connections within the splenium in sighted subjects are topographically organized: tracts projecting

across the dorsal-to-ventral direction in visual cortex are orthogonal to tracts projecting across the anterior-to-posterior direction. We found no disruption of topographic organization within either early blind or anophthalmic subjects, suggesting that neither prenatal retinal activity nor postnatal visual experience play a major role in determining the gross topographic organization of visual callosal axons within the splenium.

Previous studies (Dougherty et al., 2005; Saenz and Fine, 2010) proposed that fibers from dorsal visual areas project to the superior-caudal end of the splenium and fibers from ventral visual areas project to the inferior-rostral corner of the splenium, which would result in vectors oriented at ~135 degrees. However our quantification across a larger number of sighted subjects suggests a mapping whereby fibers from dorsal visual areas tend to project to the caudal end of the splenium and fibers from ventral visual areas tend to project to the rostral corner of the splenium, with a resulting vector oriented at ~100 degrees. A previous study suggested (Saenz and Fine, 2010) that fibers from anterior visual areas projected to the inferior-caudal splenium while fibers from posterior visual areas projected to the superior-rostral corner of the splenium, resulting in vectors oriented at ~45 degrees. In contrast, our quantification suggests a projection whereby fibers from anterior visual areas project to the inferior portion of splenium, while fibers from posterior visual areas project to the superior portion of the splenium, with a resulting vector oriented at ~8 degrees. Note that these small differences in map orientation compared to previous studies may partially result from methodological differences in the orientation of the callosum (e.g. AC-PC vs. callosal alignment). To avoid potential complications with reorienting diffusion vectors, we choose not to AC-PC align our diffusion volumes and instead carried out all measurements in the native diffusion space. Also, since our main focus was on the topography of connections within the callosum itself, we choose to use the callosum as our common frame of reference, as opposed to an alternative anatomical location outside the callosum (e.g. AC-PC vector).

4.4 Comparison of our data to animal models

Although, to our knowledge, this is the first study to examine the effects of visual deprivation on retinotopic organization within the splenium itself, there is a large animal literature describing the effects of early vision loss on visual cortico-cortico connections (Bock et al., 2012; Bock and Olavarria, 2011; Bock et al., 2010; Olavarria and Hiroi, 2003; for review, see Innocenti, 1991; Innocenti and Price, 2005). In these studies, it is consistently found that the pattern of callosal connections at the level of cortex is perturbed due to early visual deprivation, including the spreading of these callosal connections into cortical areas that are acallosal in sighted control animals. However, the extent of disruption seems to be local – often on the order of microns. Indeed, consistent with our findings, major topographical features, including the restriction of callosal fibers to the border between visual areas representing the vertical meridian, can still be recognized in animals lacking visual input (Bock et al., 2012; Bock and Olavarria, 2011; Bock et al., 2010; Dehay et al., 1989; Olavarria et al., 1987; Olavarria and Van Sluyters, 1995). Thus, the effects of enucleation may perhaps be better described as a change in specificity or local topography around normal callosal territory rather than a complete topographical reorganization. For example, data from Olavarria et al. (2008) and Fish et al. (1991) have suggested that enucleation leads to larger axonal terminal arborization, and Bock & Olavarria (2011) found that enucleation leads to a decrease in the precision of visual cortico-cortical connections. The *in vivo* diffusion methods used here can only map large scale splenial fiber organization, on the order of millimeters, limiting our ability to comment on more local changes in topographical organization.

While it is perfectly consistent with our data that retinotopic disruption within the splenium occurs at a scale not observable using current diffusion tractography techniques, our results do demonstrate that large-scale retinotopic organization within the splenium is robust to loss

of pre- and postnatal retinal input. Further support for the notion that the gross topographical organization of visual connections remains largely undisturbed by visual deprivation comes from animal studies. A recent paper in the mouse by Charbonneau et al. (2012) found little to no difference in the strength nor in the laminar distribution of cortical and subcortical projections to V1 between anophthalmic, enucleated, and sighted mice. Another recent paper in the rat by Chan et al. (2012) found no difference in diffusivity, including FA, radial and longitudinal diffusivity, within the splenium of the corpus callosum in monocularly deprived as well as monocularly and binocularly enucleated animals. Finally, a study in anophthalmic mice (Kaiserman-Abramof et al., 1980) showed that despite the lack of retinal afferents and a reduction of its neuronal population to 76% of normal, the dorsal lateral geniculate nucleus projects to area 17 in an essentially normal topographic pattern.

Animal studies have also shown that prenatal retinal activity and postnatal visual experience are only required for later stages of cortical wiring in the visual pathway (Katz and Shatz, 1996). Molecular mechanisms seem to be the primary influence on axon pathfinding early in development (Goodman and Shatz, 1993; Katz and Crowley, 2002; Katz and Shatz, 1996; Lopez-Bendito and Molnar, 2003; Price et al., 2006; Ruthazer and Cline, 2004; Sur and Rubenstein, 2005) with neuronal activity only playing a role in shaping the wiring of connections significantly later in life.

4.4 Callosal projections develop before the onset of retinal waves

Currently, in human and macaque, the timing of many visual callosal events, such as the generation of visual callosal axons, their crossing of the midline, arrival to the contralateral white matter, and the invasion of the cortical plate, have not been experimentally characterized in any great detail. However, while there are known species differences, the order and timing of neurogenesis (Finlay and Darlington, 1995) and axon extension and projection segregation (Darlington et al., 1999) show consistent patterns across mammalian species, thereby allowing the development of a statistical model for the extrapolation of timelines across species, which includes an estimated timeline for humans (Clancy et al., 2007a; Clancy et al., 2007b).

As described in **Figure 5**, according to this model, the first visual callosally projecting axons are generated at embryonic day 89.4 and cross the midline at E100. The onset of retinal waves occurs at E101.2, *after* visual callosal axons cross the midline and prior to LGN axons innervating cortical layer IV, which occurs at E132.1. Visual callosal axons reach contralateral white matter by E154.1, but estimates suggest that these axons do not invade the cortical plate for another 16-30 days (Aggoun-Zouaoui and Innocenti, 1994; Fish et al., 1991; Kroenke et al., 2009; Kroenke et al., 2007; Mizuno et al., 2007). One possible explanation for this ‘waiting period’ is that activity patterns within the retinae during this time dictate the pattern of innervation of cortex. Support for this hypothesis comes from Olavarria & Hiroi (2003), who showed in both rat and mouse that the development of retinotopically-matched callosal linkages depends critically on retinal influences during this ‘waiting period’. Given that retinal activity begins *after* visual callosal axons cross the midline, but *before* they innervate cortex, our results combined with the animal literature suggest that the topography of callosal axons within the splenium develops and is maintained in an activity-independent manner based on molecular mechanisms, with separate activity-dependent mechanisms specifying callosal topography at the level of cortex.

4.5. Conclusions

In summary, while previous studies (Dehay et al., 1989; Hoffmann et al., 2012) have suggested that the gross organization of visual callosal tracts is determined and maintained

in an activity-independent manner by molecular mechanisms early in development, our results are the first to demonstrate that the retinotopic organization of fibers within these tracts is similarly robust to altered visual experience. These results suggest that topographical disruption of cortico-cortical connections that have been described (for review, see Innocenti, 1991; Innocenti and Price, 2005) as a result of blindness likely occur as white matter connections innervate cortex, rather than within the tracts themselves. While we have demonstrated that large-scale topography remains intact, future studies with more power will be required to determine how tissue properties within this tract (e.g. myelination, axon diameter) are affected by altered visual experience.

Supplementary Material

Refer to Web version on PubMed Central for supplementary material.

Acknowledgments

We wish to thank all subjects involved for their cooperation during this study. This work was supported by NIH Grant EY014645 (I.F.) and a Royal Society University Research Fellowship (H.B.).

References

- Aggoun-Zouaoui D, Innocenti GM. Juvenile Visual Callosal Axons in Kittens Display Origin-Related and Fate-Related Morphology and Distribution of Arbors. *European Journal of Neuroscience*. 1994; 6:1846–1863. [PubMed: 7704296]
- Ashburner J, Andersson JL, Friston KJ. Image registration using a symmetric prior--in three dimensions. *Human Brain Mapping*. 2000; 9:212–225. [PubMed: 10770230]
- Ashburner J, Friston KJ. Why voxel-based morphometry should be used. *Neuroimage*. 2001; 14:1238–1243. [PubMed: 11707080]
- Behrens TE, Berg HJ, Jbabdi S, Rushworth MF, Woolrich MW. Probabilistic diffusion tractography with multiple fibre orientations: What can we gain? *Neuroimage*. 2007; 34:144–155. [PubMed: 17070705]
- Behrens TE, Woolrich MW, Jenkinson M, Johansen-Berg H, Nunes RG, Clare S, Matthews PM, Brady JM, Smith SM. Characterization and propagation of uncertainty in diffusion-weighted MR imaging. *Magn Reson Med*. 2003a; 50:1077–1088. [PubMed: 14587019]
- Behrens TEJ, Johansen-Berg H, Woolrich MW, Smith SM, Wheeler-Kingshott CAM, Boulby PA, Barker GJ, Sillery EL, Sheehan K, Ciccarelli O, Thompson AJ, Brady JM, Matthews PM. Non-invasive mapping of connections between human thalamus and cortex using diffusion imaging. *Nature Neuroscience*. 2003b; 6:750–757.
- Benjamini Y, Hochberg Y. Controlling the False Discovery Rate - a Practical and Powerful Approach to Multiple Testing. *Journal of the Royal Statistical Society Series B-Methodological*. 1995; 57:289–300.
- Bock AS, Kroenke CD, Taber EN, Olavarria JF. Retinal input influences the size and corticocortical connectivity of visual cortex during postnatal development in the ferret. *J Comp Neurol*. 2012; 520:914–932. [PubMed: 21830218]
- Bock AS, Olavarria JF. Neonatal enucleation during a critical period reduces the precision of cortico-cortical projections in visual cortex. *Neuroscience Letters*. 2011; 501:152–156. [PubMed: 21782890]
- Bock AS, Olavarria JF, Leigland LA, Taber EN, Jespersen SN, Kroenke CD. Diffusion tensor imaging detects early cerebral cortex abnormalities in neuronal architecture induced by bilateral neonatal enucleation: an experimental model in the ferret. *Front Syst Neurosci*. 2010; 4:149. [PubMed: 21048904]
- Bridge H, Cowey A, Ragge N, Watkins K. Imaging studies in congenital anophthalmia reveal preservation of brain architecture in ‘visual’ cortex. *Brain*. 2009; 132:3467–3480. [PubMed: 19892766]

- Chalupa LM. Retinal waves are unlikely to instruct the formation of eye-specific retinogeniculate projections. *Neural Dev.* 2009; 4:25. [PubMed: 19580684]
- Chan KC, Cheng JS, Fan S, Zhou IY, Yang J, Wu EX. In vivo evaluation of retinal and callosal projections in early postnatal development and plasticity using manganese-enhanced MRI and diffusion tensor imaging. *Neuroimage.* 2012; 59:2274–2283. [PubMed: 21985904]
- Charbonneau V, Laramee ME, Boucher V, Bronchti G, Boire D. Cortical and subcortical projections to primary visual cortex in anophthalmic, enucleated and sighted mice. *Eur J Neurosci.* 2012
- Clancy B, Finlay BL, Darlington RB, Anand KJ. Extrapolating brain development from experimental species to humans. *Neurotoxicology.* 2007a; 28:931–937. [PubMed: 17368774]
- Clancy B, Kersh B, Hyde J, Darlington RB, Anand KJ, Finlay BL. Web-based method for translating neurodevelopment from laboratory species to humans. *Neuroinformatics.* 2007b; 5:79–94. [PubMed: 17426354]
- Clarke S, Miklossy J. Occipital cortex in man: organization of callosal connections, related myelo- and cytoarchitecture, and putative boundaries of functional visual areas. *J Comp Neurol.* 1990; 298:188–214. [PubMed: 2212102]
- Dale AM, Fischl B, Sereno MI. Cortical surface-based analysis. I. Segmentation and surface reconstruction. *Neuroimage.* 1999; 9:179–194. [PubMed: 9931268]
- Dale AM, Sereno MI. Improved Localization of Cortical Activity by Combining EEG and MEG with MRI Cortical Surface Reconstruction: A Linear Approach. *Journal of Cognitive Neuroscience.* 1993; 5:162–176.
- Darlington RB, Dunlop SA, Finlay BL. Neural development in metatherian and eutherian mammals: variation and constraint. *J Comp Neurol.* 1999; 411:359–368. [PubMed: 10413772]
- de Lacoste MC, Kirkpatrick JB, Ross ED. Topography of the human corpus callosum. *J Neuropathol Exp Neurol.* 1985; 44:578–591. [PubMed: 4056827]
- Dehay C, Giroud P, Berland M, Killackey H, Kennedy H. Contribution of thalamic input to the specification of cytoarchitectonic cortical fields in the primate: effects of bilateral enucleation in the fetal monkey on the boundaries, dimensions, and gyrification of striate and extrastriate cortex. *J Comp Neurol.* 1996; 367:70–89. [PubMed: 8867284]
- Dehay C, Horsburgh G, Berland M, Killackey H, Kennedy H. Maturation and connectivity of the visual cortex in monkey is altered by prenatal removal of retinal input. *Nature.* 1989; 337:265–267. [PubMed: 2536139]
- Destrieux C, Fischl B, Dale A, Halgren E. Automatic parcellation of human cortical gyri and sulci using standard anatomical nomenclature. *Neuroimage.* 2010; 53:1–15. [PubMed: 20547229]
- Dougherty RF, Ben-Shachar M, Bammer R, Brewer AA, Wandell BA. Functional organization of human occipital-callosal fiber tracts. *Proc Natl Acad Sci U S A.* 2005; 102:7350–7355. [PubMed: 15883384]
- Dougherty RF, Ben-Shachar M, Deutsch GK, Hernandez A, Fox GR, Wandell BA. Temporal-callosal pathway diffusivity predicts phonological skills in children. *Proc Natl Acad Sci U S A.* 2007; 104:8556–8561. [PubMed: 17483487]
- Finlay BL, Darlington RB. Linked regularities in the development and evolution of mammalian brains. *Science.* 1995; 268:1578–1584. [PubMed: 7777856]
- Fischl B, Dale AM. Measuring the thickness of the human cerebral cortex from magnetic resonance images. *Proc Natl Acad Sci U S A.* 2000; 97:11050–11055. [PubMed: 10984517]
- Fischl B, Liu A, Dale AM. Automated manifold surgery: Constructing geometrically accurate and topologically correct models of the human cerebral cortex. *IEEE Trans Med Imaging.* 2001; 20:70–80. [PubMed: 11293693]
- Fischl B, Salat DH, Busa E, Albert M, Dieterich M, Haselgrove C, van der Kouwe A, Killiany R, Kennedy D, Klaveness S, Montillo A, Makris N, Rosen B, Dale AM. Whole brain segmentation: automated labeling of neuroanatomical structures in the human brain. *Neuron.* 2002; 33:341–355. [PubMed: 11832223]
- Fischl B, Salat DH, van der Kouwe AJ, Makris N, Segonne F, Quinn BT, Dale AM. Sequence-independent segmentation of magnetic resonance images. *Neuroimage 23 Suppl.* 2004; 1:S69–84.
- Fischl B, Sereno MI, Dale AM. Cortical surface-based analysis - II: Inflation, flattening, and a surface-based coordinate system. *Neuroimage.* 1999a; 9:195–207. [PubMed: 9931269]

- Fischl B, Sereno MI, Tootell RBH, Dale AM. High-resolution intersubject averaging and a coordinate system for the cortical surface. *Human Brain Mapping*. 1999b; 8:272–284. [PubMed: 10619420]
- Fish SE, Rhoades RW, Bennett-Clarke CA, Figley B, Mooney RD. Organization, Development and Enucleation-induced Alterations in the Visual Callosal Projection of the Hamster: Single Axon Tracing with Phaseolus vulgaris leucoagglutinin and Di-I. *Eur J Neurosci*. 1991; 3:1255–1270. [PubMed: 12106224]
- Goodman CS, Shatz CJ. Developmental Mechanisms That Generate Precise Patterns of Neuronal Connectivity. *Cell*. 1993; 72:77–98. [PubMed: 8428376]
- Graven SN. Early neurosensory visual development of the fetus and newborn. *Clin Perinatol*. 2004; 31:199–216. [PubMed: 15289028]
- Hasan KM, Alexander AL, Narayana PA. Does fractional anisotropy have better noise immunity characteristics than relative anisotropy in diffusion tensor MRI? An analytical approach. *Magnetic Resonance in Medicine*. 2004; 51:413–417. [PubMed: 14755670]
- Hinds O, Polimeni JR, Rajendran N, Balasubramanian M, Amunts K, Zilles K, Schwartz EL, Fischl B, Triantafyllou C. Locating the functional and anatomical boundaries of human primary visual cortex. *Neuroimage*. 2009; 46:915–922. [PubMed: 19328238]
- Hinds OP, Rajendran N, Polimeni JR, Augustinack JC, Wiggins G, Wald LL, Diana Rosas H, Potthast A, Schwartz EL, Fischl B. Accurate prediction of V1 location from cortical folds in a surface coordinate system. *Neuroimage*. 2008; 39:1585–1599. [PubMed: 18055222]
- Hoffmann, Michael B.; Kaule, Falko R.; Levin, N.; Masuda, Y.; Kumar, A.; Gottlob, I.; Horiguchi, H.; Dougherty, Robert F.; Stadler, J.; Wolynski, B.; Speck, O.; Kanowski, M.; Liao, Yaping J.; Wandell, Brian A.; Dumoulin, Serge O. Plasticity and Stability of the Visual System in Human Optic Chiasm. *Neuron*. 2012; 75:393–401. [PubMed: 22884323]
- Huang H, Zhang JY, Jiang HY, Wakana S, Poetscher L, Miller MI, van Zijl PCM, Hillis AE, Wytik R, Mori S. DTI tractography based parcellation of white matter: Application to the mid-sagittal morphology of corpus callosum. *Neuroimage*. 2005; 26:195–205. [PubMed: 15862219]
- Hubel DH, Wiesel TN. Cortical and callosal connections concerned with the vertical meridian of visual fields in the cat. *J Neurophysiol*. 1967; 30:1561–1573. [PubMed: 6066454]
- Huberman AD, Dehay C, Berland M, Chalupa LM, Kennedy H. Early and rapid targeting of eye-specific axonal projections to the dorsal lateral geniculate nucleus in the fetal macaque. *J Neurosci*. 2005; 25:4014–4023. [PubMed: 15843603]
- Innocenti GM. The development of projections from cerebral cortex. *Progr Sens Physiol*. 1991; 12:65–114.
- Innocenti GM, Price DJ. Exuberance in the development of cortical networks. *Nat Rev Neurosci*. 2005; 6:955–965. [PubMed: 16288299]
- Jiang J, Zhu W, Shi F, Liu Y, Li J, Qin W, Li K, Yu C, Jiang T. Thick visual cortex in the early blind. *J Neurosci*. 2009; 29:2205–2211. [PubMed: 19228973]
- Jones DK, Simmons A, Williams SC, Horsfield MA. Non-invasive assessment of axonal fiber connectivity in the human brain via diffusion tensor MRI. *Magn Reson Med*. 1999; 42:37–41. [PubMed: 10398948]
- Kaiserman-Abramof IR, Graybiel AM, Nauta WJ. The thalamic projection to cortical area 17 in a congenitally anophthalmic mouse strain. *Neuroscience*. 1980; 5:41–52. [PubMed: 7366842]
- Katz LC, Crowley JC. Development of cortical circuits: lessons from ocular dominance columns. *Nat Rev Neurosci*. 2002; 3:34–42. [PubMed: 11823803]
- Katz LC, Shatz CJ. Synaptic activity and the construction of cortical circuits. *Science*. 1996; 274:1133–1138. [PubMed: 8895456]
- Kennedy H, Dehay C, Bullier J. Organization of the callosal connections of visual areas V1 and V2 in the macaque monkey. *J Comp Neurol*. 1986; 247:398–415. [PubMed: 3088065]
- Kroenke CD, Taber EN, Leigland LA, Knutsen AK, Bayly PV. Regional patterns of cerebral cortical differentiation determined by diffusion tensor MRI. *Cereb Cortex*. 2009; 19:2916–2929. [PubMed: 19363145]
- Kroenke CD, Van Essen DC, Inder TE, Rees S, Bretthorst GL, Neil JJ. Microstructural changes of the baboon cerebral cortex during gestational development reflected in magnetic resonance imaging diffusion anisotropy. *J Neurosci*. 2007; 27:12506–12515. [PubMed: 18003829]

- Lepore N, Voss P, Lepore F, Chou YY, Fortin M, Gougoux F, Lee AD, Brun C, Lassonde M, Madsen SK, Toga AW, Thompson PM. Brain structure changes visualized in early- and late-onset blind subjects. *Neuroimage*. 2010; 49:134–140. [PubMed: 19643183]
- Levin N, Dumoulin SO, Winawer J, Dougherty RF, Wandell BA. Cortical maps and white matter tracts following long period of visual deprivation and retinal image restoration. *Neuron*. 2010; 65:21–31. [PubMed: 20152110]
- Lopez-Bendito G, Molnar Z. Thalamocortical development: how are we going to get there? *Nat Rev Neurosci*. 2003; 4:276–289. [PubMed: 12671644]
- Mizuno H, Hirano T, Tagawa Y. Evidence for activity-dependent cortical wiring: Formation of interhemispheric connections in neonatal mouse visual cortex requires projection neuron activity. *Journal of Neuroscience*. 2007; 27:6760–6770. [PubMed: 17581963]
- Olavaria J, Malach R, Van Sluyters RC. Development of visual callosal connections in neonatally enucleated rats. *J Comp Neurol*. 1987; 260:321–348. [PubMed: 3597836]
- Olavaria JF. Non-mirror-symmetric patterns of callosal linkages in areas 17 and 18 in cat visual cortex. *J Comp Neurol*. 1996; 366:643–655. [PubMed: 8833114]
- Olavaria JF, Hiroi R. Retinal influences specify cortico-cortical maps by postnatal day six in rats and mice. *J Comp Neurol*. 2003; 459:156–172. [PubMed: 12640667]
- Olavaria JF, Laing R, Hiroi R, Lasiene J. Topography and axon arbor architecture in the visual callosal pathway: effects of deafferentation and blockade of N-methyl-D-aspartate receptors. *Biol Res*. 2008; 41:413–424. [PubMed: 19621122]
- Olavaria JF, Van Sluyters RC. Overall pattern of callosal connections in visual cortex of normal and enucleated cats. *J Comp Neurol*. 1995; 363:161–176. [PubMed: 8642068]
- Pandya DN, Karol EA, Heilbronn D. The topographical distribution of interhemispheric projections in the corpus callosum of the rhesus monkey. *Brain Res*. 1971; 32:31–43. [PubMed: 5000193]
- Payne BR, Siwek DF, Lomber SG. Complex transcalsal interactions in visual cortex. *Vis Neurosci*. 1991; 6:283–289. [PubMed: 2054329]
- Price DJ, Kennedy H, Dehay C, Zhou L, Mercier M, Jossin Y, Goffinet AM, Tissir F, Blakey D, Molnar Z. The development of cortical connections. *Eur J Neurosci*. 2006; 23:910–920. [PubMed: 16519656]
- Rockland KS, Lund JS. Intrinsic laminar lattice connections in primate visual cortex. *J Comp Neurol*. 1983; 216:303–318. [PubMed: 6306066]
- Rockland KS, Pandya DN. Topography of occipital lobe commissural connections in the rhesus monkey. *Brain Res*. 1986; 365:174–178. [PubMed: 3947983]
- Ruthazer ES, Cline HT. Insights into activity-dependent map formation from the retinotectal system: a middle-of-the-brain perspective. *J Neurobiol*. 2004; 59:134–146. [PubMed: 15007832]
- Saenz M, Fine I. Topographic organization of V1 projections through the corpus callosum in humans. *Neuroimage*. 2010; 52:1224–1229. [PubMed: 20553894]
- Segonne F, Dale AM, Busa E, Glessner M, Salat D, Hahn HK, Fischl B. A hybrid approach to the skull stripping problem in MRI. *Neuroimage*. 2004; 22:1060–1075. [PubMed: 15219578]
- Segonne F, Pacheco J, Fischl B. Geometrically accurate topology-correction of cortical surfaces using nonseparating loops. *IEEE Trans Med Imaging*. 2007; 26:518–529. [PubMed: 17427739]
- Segraves MA, Rosenquist AC. The Afferent and Efferent Callosal Connections of Retinotopically Defined Areas in Cat Cortex. *Journal of Neuroscience*. 1982; 2:1090–1107. [PubMed: 6180150]
- Shimony JS, Burton H, Epstein AA, McLaren DG, Sun SW, Snyder AZ. Diffusion tensor imaging reveals white matter reorganization in early blind humans. *Cereb Cortex*. 2006; 16:1653–1661. [PubMed: 16400157]
- Sled JG, Zijdenbos AP, Evans AC. A nonparametric method for automatic correction of intensity nonuniformity in MRI data. *IEEE Trans Med Imaging*. 1998; 17:87–97. [PubMed: 9617910]
- Stevenson, RE. Human malformations and related anomalies. 2nd ed.. Oxford University Press; Oxford ; New York: 2006.
- Sur M, Rubenstein JL. Patterning and plasticity of the cerebral cortex. *Science*. 2005; 310:805–810. [PubMed: 16272112]

- Takao H, Hayashi N, Ohtomo K. Effect of scanner in asymmetry studies using diffusion tensor imaging. *Neuroimage*. 2011; 54:1053–1062. [PubMed: 20850553]
- Van Essen DC, Newsome WT, Bixby JL. The pattern of interhemispheric connections and its relationship to extrastriate visual areas in the macaque monkey. *J Neurosci*. 1982; 2:265–283. [PubMed: 7062108]
- Wiesel TN, Hubel DH. Comparison of the effects of unilateral and bilateral eye closure on cortical unit responses in kittens. *J Neurophysiol*. 1965a; 28:1029–1040. [PubMed: 5883730]
- Wiesel TN, Hubel DH. Extent of recovery from the effects of visual deprivation in kittens. *J Neurophysiol*. 1965b; 28:1060–1072. [PubMed: 5883732]
- Yu C, Shu N, Li J, Qin W, Jiang T, Li K. Plasticity of the corticospinal tract in early blindness revealed by quantitative analysis of fractional anisotropy based on diffusion tensor tractography. *Neuroimage*. 2007; 36:411–417. [PubMed: 17442594]

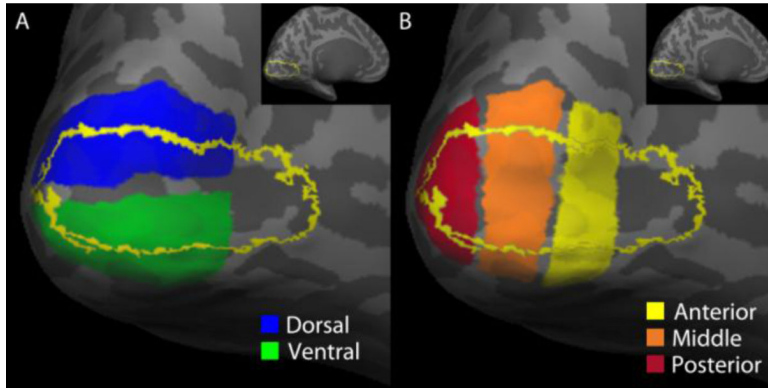


Figure 1. Definition of occipital ROIs

Left hemisphere cortical surface of a sighted subject showing the (A) dorsal (blue) and ventral (green) ROIs, as well as (B) the anterior (yellow), middle (orange), and posterior (red) ROIs. The yellow line in (A) and (B) represents the border of V1, defined by Freesurfer (see methods). The V1 ROI included the following cortical labels: 2 – G_and_S_occipital_inf ; 11 – G_cuneus ; 19 – G_occipital_middle ; 20 – G_occipital_sup ; 21 – G_oc-temp_lat-fusifor ; 22 – G_oc-temp_med-Lingual ; 43 – Pole_occipital ; 45 – S_calcarine ; 52 – S_collat_transv_post ; 58 – S_oc_middle_and_Lunatus ; 59 – S_oc_sup_and_transversal ; 60 – S_occipital_ant ; 61 – S_oc-temp_lat ; 62 – S_oc-temp_med_and_Lingual ; 66 – S_parieto_occipital (see (Destrieux et al., 2010) for label details). Insets show V1 from a medial view of the entire brain to aid in orienting the reader.

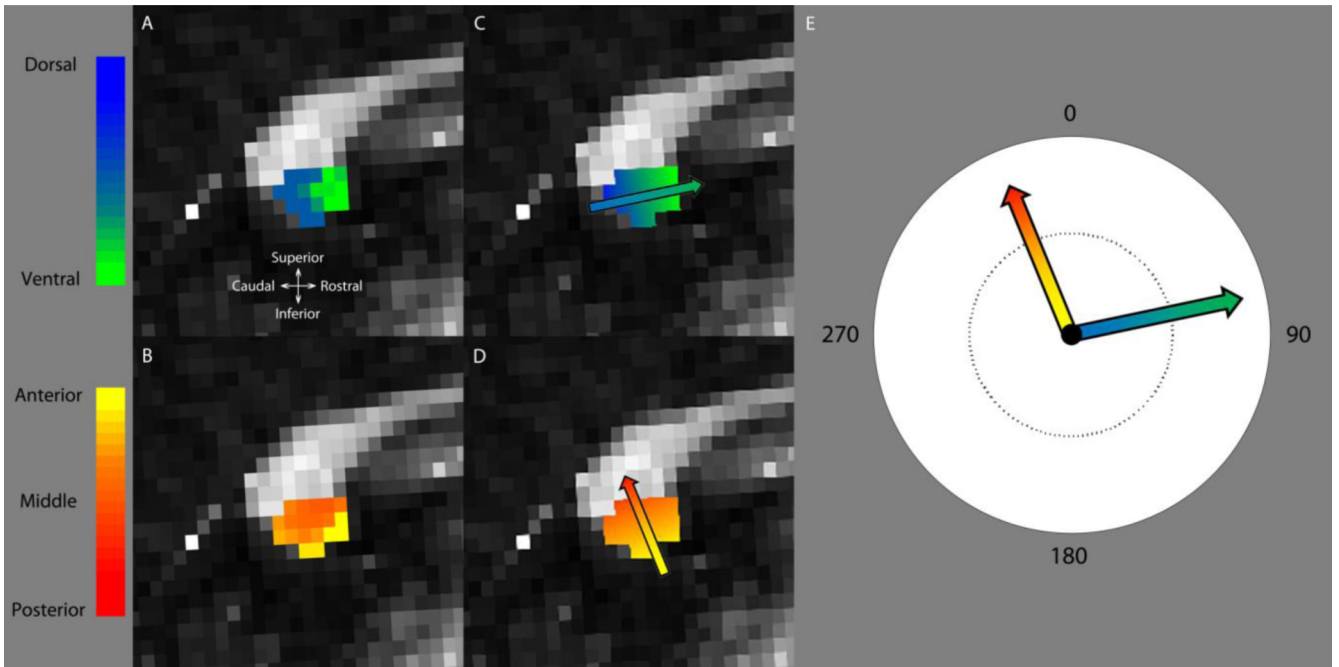


Figure 2. Calculation of projection probabilities

Splenic probabilistic maps for a single sighted subject, showing the (A) dorsal/ventral and (B) anterior/posterior maps. Anatomical directions are shown in (A). We used color maps where dorsal = blue [0 0 1] and ventral = green [0 1 0] such that if a voxel had a connectivity value of 0.9 to the ventral region and 0.1 to the dorsal region then it was assigned a green color value of $0.9 * [0 1 0] + 0.1 * [0 0 1]$. The anterior-to-posterior classification was likewise labeled using a yellow-red scale: anterior = yellow [1 1 0], middle = orange [1 0.5 0], and posterior = red [1 0 0]. A linear ramp was fit to each map, shown in (C) and (D), resulting in a vector that represents the orientation (vector angle) and gradient (vector line length) of the (C) dorsal-to-ventral and (D) anterior-to-posterior splenic maps. A polar plot summarizing the resulting vectors for each map is found in (E).

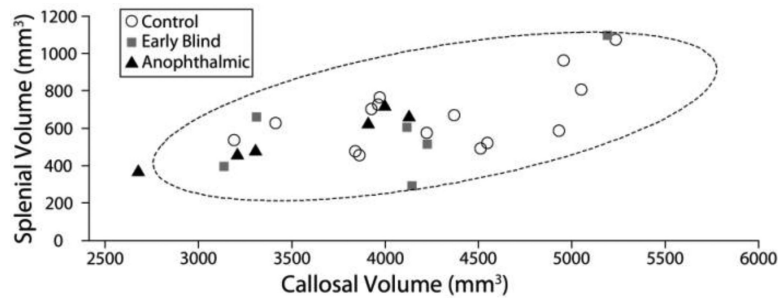


Figure 3. Splenial and Callosal Volume

Scatter plot of the occipital callosal fiber volume in relation to the volume of the corpus callosum. While blind subjects tended to have relatively small callosal volumes as compared to sighted subjects, all but one anophthalmic subject fell within the normal range, as represented by a 2 standard deviation covariance ellipsoid (dotted line).

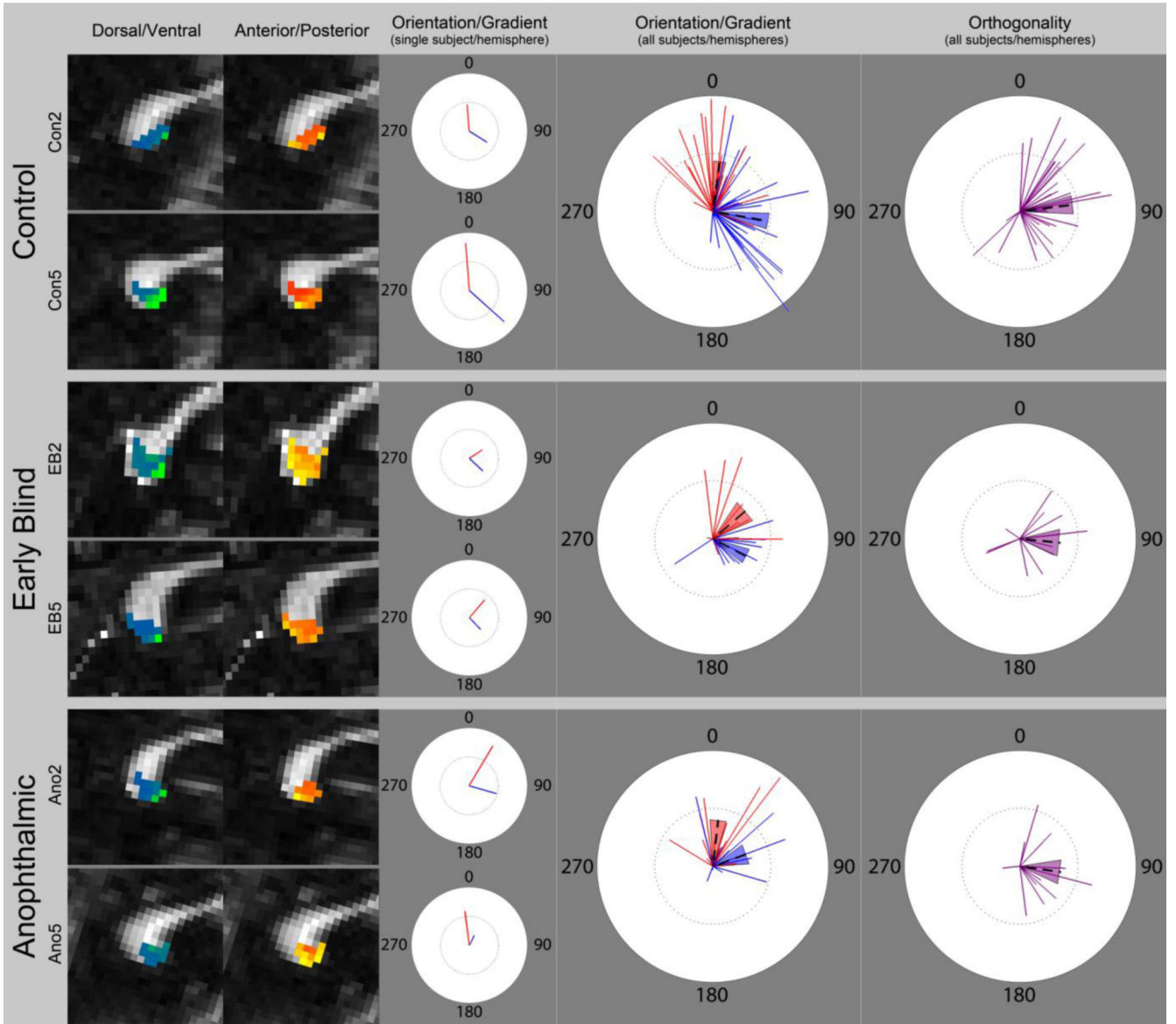


Figure 4. Summary polar plots

Left column: data from the left hemisphere of two control, two early blind, and two anophthalmic subjects. *Individual Vector Plots:* vectors representing the dorsal/ventral (blue) and anterior/posterior (red) maps for subjects in the left column. *Summary Vector Plots:* vectors representing maps from all subjects (both hemispheres) for each group; dashed lines indicate the average slope and orientation; shaded regions represent the standard error of the mean. *Summary Orthogonality Plots:* difference between the two map vectors (purple) for each subject (both hemispheres); lengths of lines indicate the average slope of the dorsal/ventral and anterior/posterior maps. In all other vector plots, lengths of lines indicate the slope of the gradient for that map, numbers indicate the orientation angle in degrees, inner dotted circles indicate a slope of 0.005, and outer circles indicate a slope of 0.01.

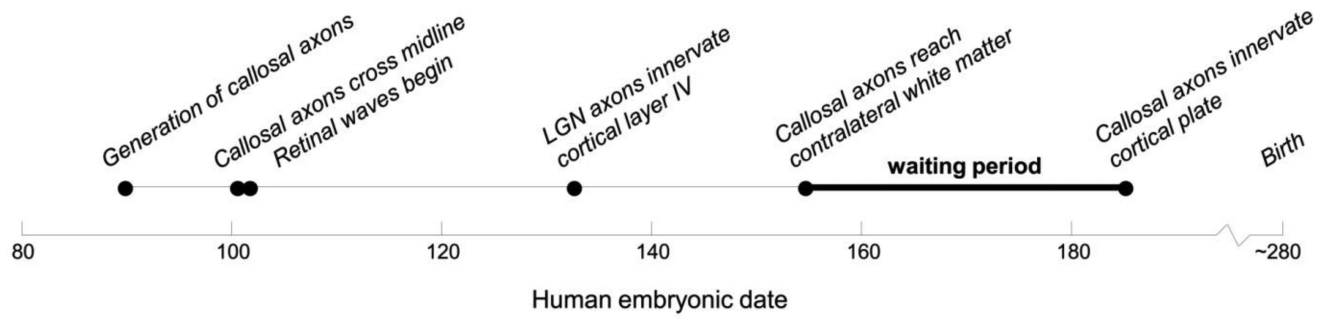


Figure 5. Timeline of human visual development

Dates are based on human and laboratory animal data (Clancy et al., 2007b).

Table 1

Brief subject descriptions

Subject	Gender	Age	Clinical description
EB1	F	61	Right eye ruptured at 2 months, detached retina at 5 years; no light perception
EB2	F	51	Retinopathy of prematurity; low light perception until retina detached at 25 years; 2 months premature
EB3	M	59	Retinopathy of prematurity; no light perception; 2 months premature
EB4	M	60	Retinopathy of prematurity; no light perception; 2 months premature
EB5	F	36	Retinopathy of prematurity; low light perception until 14 years; 2 months premature
EB6	M	30	Leber's congenital amaurosis; low light perception
Ano1	M	28	Bilateral anophthalmia associated with OTX2 mutation; mother carrier; delayed speech and motor development
Ano2	F	31	Isolated bilateral anophthalmia; family history of microphthalmia
Ano3	M	18	Isolated bilateral anophthalmia associated with dysplastic kidneys and mild systolic murmur; no family history
Ano4	F	20	Isolated bilateral anophthalmia, right with orbital cyst; no family history
Ano5	M	23	Isolated bilateral anophthalmia; no family history
Ano6	M	25	Isolated bilateral anophthalmia; no family history

Age is at time of scan.

Table 2

No difference in callosal or splenial volume across subject groups.

	Control		Early blind		Anophthalmic		p-value
	mean	s.d.	mean	s.d.	mean	s.d.	
Callosal volume (mm ³)	4267.47	606.21	4021.92	737.61	3538.67	565.90	0.075
Splenial volume (mm ³)	666.05	179.97	594.85	282.06	550.67	135.99	0.46
Callosal area (mm ²)	663.76	74.14	576.55	85.04	660.67	113.71	0.12
Splenial area (mm ²)	88.09	15.14	78.60	23.45	88.00	26.41	0.59
Splenial/Callosal Ratio (volume)	0.16	0.03	0.15	0.05	0.15	0.02	0.85
Splenial/Callosal Ratio (area)	0.13	0.03	0.14	0.05	0.13	0.03	0.93

Callosal and splenial anatomical measurements were compared using a 1-way ANOVA. P-values shown have not undergone any post-hoc correction for multiple comparisons.

Table 3

Diffusivity measurements across subject groups.

	Control (UW)		Early blind (UW)		Control (Oxford)		Anophthalmic (Oxford)		Correction for Multiple Comparisons (16 comparisons)	
	mean	s.d.	mean	s.d.	mean	p-value	mean	s.d.	p-value	
Callosal FA	0.59	0.020	0.56	0.051	0.57	0.083	0.55	0.026	0.21	
Splenic FA	0.71	0.035	0.68	0.074	0.65	0.36	0.68	0.041	0.40	
Callosal LI ($\mu\text{m}^2/\text{msec}$)	1.60	0.055	1.57	0.11	1.84	0.45	1.82	0.043	0.69	
Splenic LI ($\mu\text{m}^2/\text{msec}$)	1.68	0.15	1.69	0.18	1.98	0.91	1.78	0.088	0.11	<i>n.s. H-B p<0.05 FDR</i>
Callosal L23 ($\mu\text{m}^2/\text{msec}$)	0.58	0.035	0.62	0.091	0.72	0.19	0.75	0.050	0.10	0.47
Splenic L23 ($\mu\text{m}^2/\text{msec}$)	0.44	0.057	0.48	0.068	0.65	0.25	0.53	0.050	0.10	0.027
Callosal MD ($\mu\text{m}^2/\text{msec}$)	0.92	0.037	0.94	0.083	1.09	0.55	1.11	0.043	0.098	0.70
Splenic MD ($\mu\text{m}^2/\text{msec}$)	0.85	0.073	0.88	0.052	1.09	0.42	0.95	0.011	0.070	<i>p<0.01, H-B p<0.01 FDR</i>

Subject groups were divided according to the scanner used for data acquisition (UW or Oxford) and diffusivity values were compared using two-sample t-tests.

P-values shown are before any post-hoc correction. Only the Splenic MD was significantly different after correction for multiple comparisons (16 groups, based on all the comparisons of this table). P-values after correction for multiple comparisons using Holm-Bonferroni (H-B) and False Discovery Rate (FDR, based on Benjamini & Hochberg (1995) are also reported.

Table 4

No difference in splenial topography

	Control		Early blind		Anophthalmic		Correction for Multiple Comparisons (4 comparisons)	
	mean	s.d.	mean	s.d.	mean	s.d.	p-value	
Dorsal-to-Ventral Orientation (degrees)	99.77	44.30	117.63	40.12	69.99	55.99	0.12	
Anterior-to-Posterior Orientation (degrees)	7.79	38.61	49.58	55.14	6.58	34.76	0.064	
Dorsal-to-Ventral Gradient	0.0048	0.0024	0.0033	0.0013	0.0031	0.0023	0.033	<i>n.s.</i> <i>H-B</i> <i>n.s.</i> <i>FDR</i>
Anterior-to-Posterior Gradient	0.0044	0.0026	0.0038	0.0022	0.0040	0.0025	0.79	
Orthogonality (degrees)	84.10	44.53	92.49	37.76	96.06	48.09	0.75	

Subject groups were compared using a 1-way ANOVA for gradients and the circular equivalent of a 1-way ANOVA (Watson-Williams multi-sample test) for angular data. P-values shown are before any post-hoc correction. P-values after correction for multiple comparisons using Holm-Bonferroni (H-B) and False Discovery Rate (FDR, based on Benjamini & Hochberg (1995)) are also reported. Dashed line indicates orthogonality is not an independent measure and is not included in post-hoc correction.